European Conference on Computational Fluid Dynamics
ECCOMAS CFD 2006
P. Wesseling, E. Oñate and J. Périaux (Eds)

DIRECT NUMERICAL SIMULATION AND LARGE-EDDY SIMULATION OF WAKE VORTICES: GOING FROM LABORATORY CONDITIONS TO FLIGHT CONDITIONS

G. Winckelmans and R. Cocle, L. Dufresne†, R. Capart*, L. Bricteux, G. Daeninck, T. Lonfils, M. Duponcheel, O. Desenfans, L. Georges*

Université catholique de Louvain (UCL), Mechanical Engng. Dept., Division TERM,
and Center for Systems Engineering and Applied Mechanics (CESAME)
Place du Levant, 2 - 1348 Louvain-la-Neuve, Belgium
e-mail: winckelmans@term.ucl.ac.be, web: http://www.term.ucl.ac.be
*now at CENAERO, CFD-Multiphysics Group
Avenue Jean Mermoz, 31 - 6041 Gosselies, Belgium
†now at Ecole de Technologie Supérieure (ETS), Mechanical Engng. Dept.
Rue Notre-Damme Ouest, 1100 - Montréal H3C 1K3, Québec, Canada

Key words: Direct Numerical Simulation, Large-Eddy Simulation, wake vortices, subgrid scale modelling, multiscale models, instabilities, ground effects

Abstract. *This paper aims at presenting DNS and LES as applied to the simulation of vortex wakes: in laboratory conditions (moderate to medium Reynolds numbers) and up to real aircraft conditions (high to very high Reynolds numbers). Only incompressible flows are considered. DNS and LES are able to capture complex 3-D physics provided one uses high quality numerical methods: methods with negligible numerical dissipation (i.e., methods that conserve energy in absence of viscosity and/or subgrid modelling) and with low dispersion errors (to properly transport complex vortical structures). Methods that can do that are: spectral methods, high order finite difference methods, and vortex-in-cell (VIC) methods. As the problems of interest are of large spatial extent and contain vortices with small cores, it is also essential that the methods be efficiently parallelized. As to LES of wake vortex flows, this require subgrid scale (SGS) models that are essentially inactive during the gentle, well-resolved, phases of the flow and within the vortex cores, and that become active only during the complex turbulent phases of the flow. The recent multiscale models, that act solely on the high wavenumbers modes of the LES, are seen to be most appropriate. We present some illustrative examples of DNS and LES results that were obtained within our group.*

1 INTRODUCTION

This paper discusses DNS and LES as applied to complex 3-D vortex wakes. Laboratory conditions involve moderate to medium Reynolds numbers while real aircraft

conditions concern high to very high Reynolds numbers. We only consider simulations of incompressible vortex flows. The numerical methods used must be of the highest quality. The methods must have negligible, if any, numerical dissipation, thus conserve energy in absence of viscosity and subgrid scale modelling. Indeed, one cannot accept uncontrolled numerical dissipation. The methods should also have low dispersion errors, as one needs to transport properly complex vorticity field. One also needs a sufficiently fine grid (i.e., a sufficient "inertial" range captured in the simulation). For LES, the subgrid-scale (SGS) models must have a good spectral behavior. One cannot accept dissipation "at all scales" nor dissipation of the vortex cores. There is also the need to properly capture the dynamics of unstable transitional flows. Hence, one needs SGS models that are essentially inactive during the gentle, well-resolved, phases of the flow and within the vortex cores, and that become active only during the complex and turbulent phases of the flow. Some of the recent multiscale SGS models are found to do quite well, especially those with dissipation operator that acts solely on the high wavenumbers modes of the LES.

We also need to treat large problems: indeed, wake vortices occupy large domains and have small cores. Parallel implementation of the numerical method is thus mandatory. There are then essentially three types of methods that can be used. First, there is the classical Fourier based pseudo-spectral method, thus with periodicity in all directions: this means that the computational boxes must be taken large enough that the effects of the image vortex systems are minimized. Second, there are the high order finite difference methods, where the convection term is discretized so as to exactly conserve energy, as [1]. Hybrid methods can be used as well (e.g., Fourier in one direction and finite differences in the other two). Third, there is the vortex-in-cell method (VIC). It is a hybrid method which combines lagrangian vortex particles but with grid-based operations: Poisson solver, high order particle-grid interpolations, high order particle redistribution, diffusion, vortex stretching, etc. As the convection is done in a lagrangian way (by moving the particles), there is essentially no dispersion. When the VIC method is combined with the fast multipole method, one can also simulate very efficiently open flow problems such as wake vortices, see [2, 3]

What about unsteady "Reynolds averaged Navier Stokes" (URANS) simulation for studying wake vortices? URANS amounts to 2-D (or quasi 3-D) simulations. It can be used in some cases as well, provided it is properly corrected for rotation and curvature effects; it however fails to properly capture complex interactions, such as the unstable vortex merging of co-rotating vortices (through 3-D instabilities), the vortex reconnection between opposite sign (and sometimes different strength) vortices, or even wake vortices interacting with a ground and its associated decay (also mostly due to 3-D effects). URANS is not addressed in this paper.

2 EXAMPLE OF DNS: A CASE WITH WAKE VORTICES IN GROUND EFFECT

Direct Numerical Simulation (DNS) of wake vortices is first considered. It is limited to low to moderate Reynolds numbers: typically for $Re = \Gamma_0/\nu$ up to 5000, with Γ_0 the total circulation of one of the wake vortices and ν the kinematic viscosity. This corresponds to vortices with significant diffusion of the vortex cores, as those obtained in laboratory conditions and at low velocity (e.g., water tank experiments on vortex pairs as those in [4]).

As an example of what can be done today, we consider DNS of a vortex pair in ground effect at $Re = 5000$ [5] (also done in support to the EC funded *FAR-Wake* project). To initialize the vortices, the algebraic profile is assumed:

$$\omega(r) = \frac{\Gamma_0}{\pi} \frac{r_c^2}{\left(r^2 + r_c^2\right)^2} , \qquad \Gamma(r) = \Gamma_0 \frac{r^2}{\left(r^2 + r_c^2\right)} , \qquad u_\theta(r) = \frac{\Gamma(r)}{2\pi\, r} . \tag{1}$$

where r_c is the effective core radius: the radius of maximum induced velocity. It is set to $0.05\, b_0$: a value typical of aircraft vortices in the far field.

The computational domain is periodic in the x (flight) and y (transverse) directions. The computational domain is $L_x = 4\, b_0$, $L_y = 8\, b_0$ and $L_z = 3\, b_0$, and the initial height of the vortex pair is b_0. The number of grid points is $N_x = 256$, $N_y = 512$ and $N_z = 256$. The grid is non-uniform in y, which allows to increase the size of the cells in the region above the vortices. A no-slip condition is set at the ground and a slip condition is set at the top of the computational domain. The simulation was run on 16 processors. The code uses fourth order finite differences. The discretization of the convective term follows [1] and conserves energy on cartesian stretched meshes: it is therefore particularly suitable for DNS and LES of turbulent flows. The Poisson equation for the pressure is solved using an efficient multigrid solver with a line Gauss-Seidel smoother. The code is designed to run efficiently in parallel.

The 2-D velocity field corresponding to the vorticity field and to the boundary conditions is evaluated numerically. A 3-D random perturbation is then added, of max amplitude equal to 1% of $u_\theta(r_c)$: this field serves as initial condition for the 3-D simulation. The descent velocity of the vortex pair out of ground effect is $V_0 = \Gamma_0/(2\pi b_0)$. This serves to define the dimensionless time $t^* = t\frac{V_0}{b_0}$.

The no-slip condition at the solid wall is at the origin of the development of boundary layers beneath the vortices, see Fig. 1.a. The boundary layers eventually separate when the primary vortices are close enough to the wall. The detached vortex-sheet then rolls-up and forms two coherent secondary vortices, see Fig. 1.b. They induce an upward velocity on the primary vortices and force the latter to rise; this is the *rebound* phenomenon. At this time, the flow is still essentially 2-D. But the secondary vortices are unstable with respect to short-wavelength modes. These perturbations are growing while the secondary vortex is orbiting around the primary vortex, see Fig. 1.c. The dipole formed by the primary

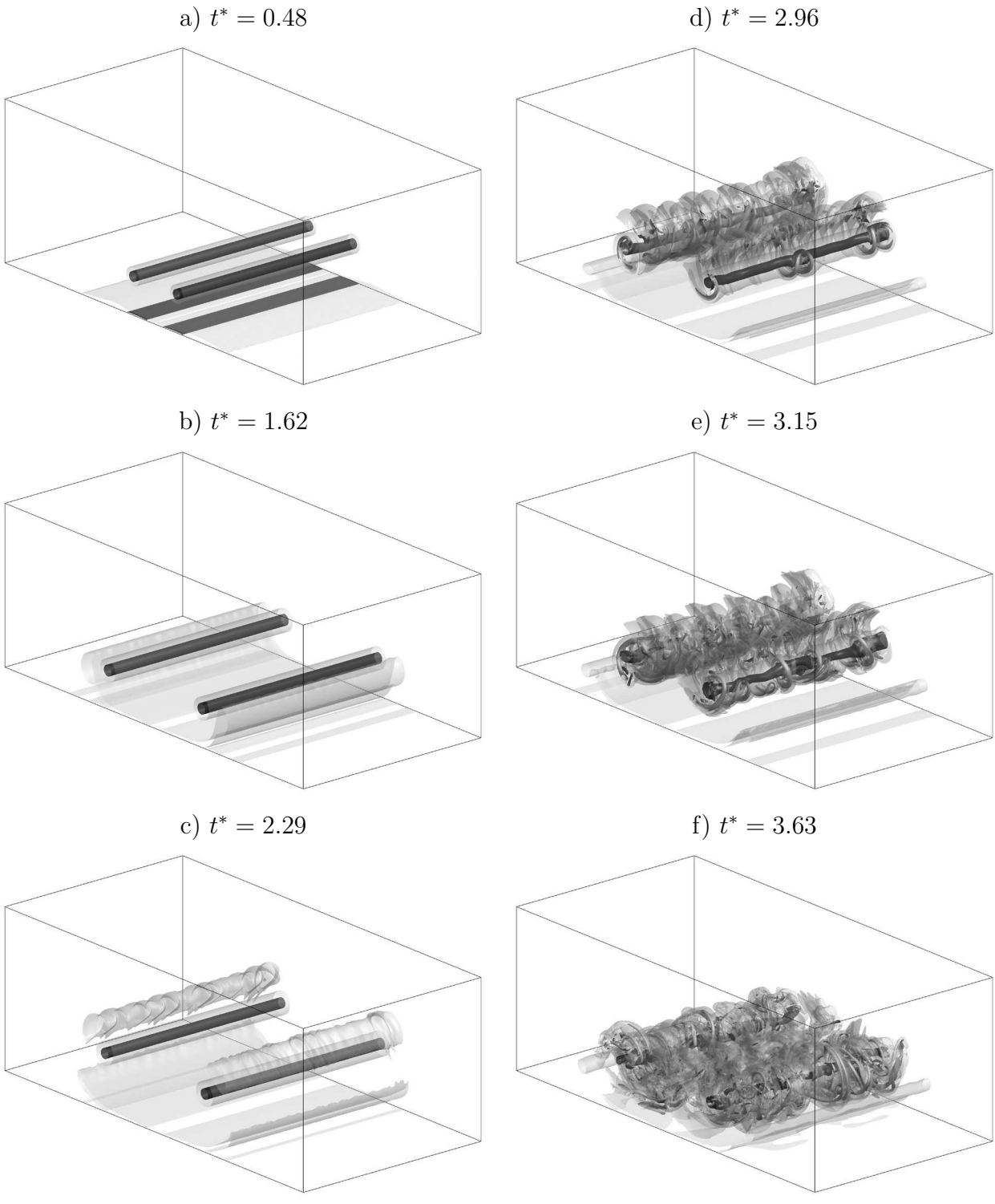

Figure 1: Visualization of the flow field using isosurfaces of $\|\vec{\omega}\| b_0^2/\Gamma_0 = 1$ and 10.

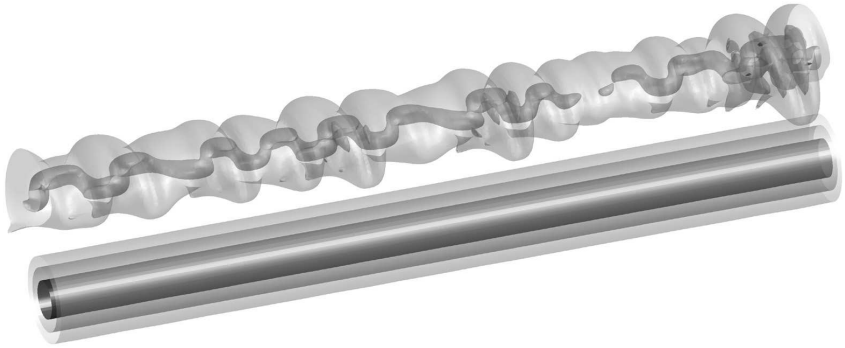

Figure 2: Visualization of the instability structure at $t^* = 2.29$ using isosurfaces of $\|\vec{\omega}\| b_0^2/\Gamma_0 = 1$, 3.5 and 10 (zoom of part of Fig. 1.c).

and secondary vortices is further shown in Fig. 2 where an additional isosurface has been drawn revealing the deformation of the core of the secondary vortex. The structure of the unstable mode is different from the results of [6]. The instability mechanism can be related to the elliptic instability of Widnall [7], also observed experimentally by [4] in the case of equal strength counter-rotating vortices at $Re \approx 2000$. It is characterized by the opposite deformation of the vortex inner core and of the outer layers, with one neutral surface in between. In the result of [6], the whole secondary vortex deformed like the core. The difference of structure is due to the higher Reynolds number (we ran a case at $Re = 2000$ and obtained the same behaviour), and also maybe to the smaller primary vortex core in our case.

The evolution of the instability and the formation of the loops (Fig. 1.d) is explained in [4] as a consequence of the structure of the deformation of the secondary vortex. Indeed, at some places, the outer layers of the secondary vortex come close enough to the primary vortex to be captured by the latter. As they orbit around it, they are stretched and their intensity increases, leading to coherent loops. These loops tend to bend the primary vortex but they don't reconnect with it. They are further stretched but new loops are created from the secondary vortex (Fig. 1.e). The flow field is now very complex and fully three-dimensional (Fig. 1.f). The secondary vortex has lost its coherence and its vorticity is distributed around the primary vortex which is itself very disturbed. The flow eventually evolves to a fully turbulent vortex system.

Fig. 3 compares the trajectories for the center of the primary vortex. Before the saturation of the secondary vortex instability, the trajectories of the 2-D and 3-D cases are identical. During the first part of the descent, they are also correctly predicted by the inviscid theory. As soon as the boundary layer starts to separate, the rebound occurs and the trajectory is significantly different from the inviscid one. After $t^* \simeq 3$, corresponding

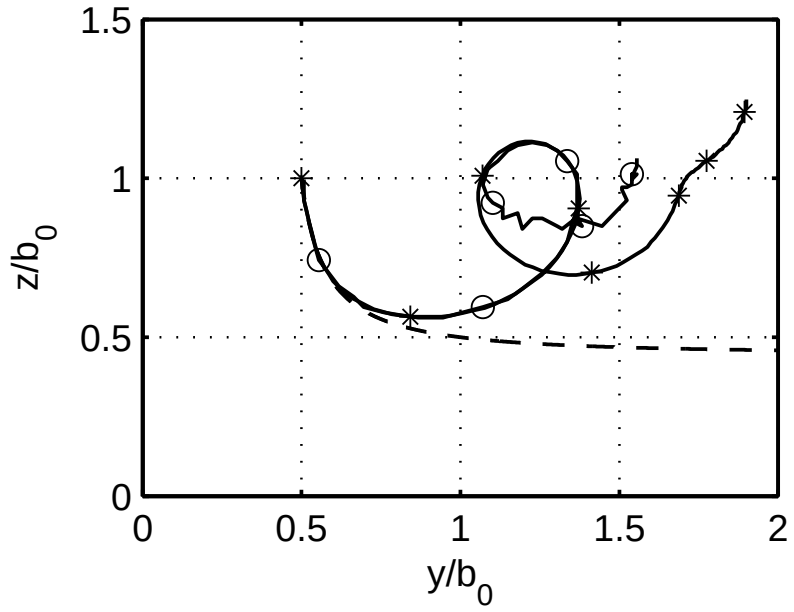

Figure 3: Trajectories of the vortices: inviscid theory (dash), 2-D ($*$) and 3-D ($\circ$) viscous simulations.

to the 3-D interaction between the secondary and primary vortices, the velocity field induced by the secondary vortex is much affected by the loss of coherence of that vortex, and the trajectory of the primary vortex is then different from the 2-D case.

The decay of the vortex system is also investigated. Different criteria exist. The kinetic energy of the global system can be used, see Fig. 4. Another usual measurement is the averaged primary vortex circulation, defined as $\Gamma_{5-15} = \frac{1}{10}\int_5^{15}\Gamma(r)\,dr$ for aircraft with a wingspan $b = 60\,[m]$, and where $\Gamma(r)$ is the circulation within a disk of radius r centered on the vortex. At the beginning, the curves of the 2-D and the 3-D cases are very close. From $t^* \simeq 2.8$, the dissipation rate in the 3-D case increases dramatically. In term of hazardousness, the 3-D instabilities are thus very beneficial. The initial 2-D decay phase is governed by the molecular viscosity. The enhanced decay is first due to three-dimensional vorticity transport during the transitional phase, and then to the abrupt generation of enstrophy when the flow becomes turbulent.

Finally, and quite importantly, we note that the beginning of the 3-D decay phase occurs later than in the simulation of [8], and also in the parameterization of [9] based on aircraft wake data. This is likely due to the moderate Reynolds number and to the smooth initial condition. To better simulate real aircraft wake conditions requires simulations at higher Reynolds number, thus using Large-Eddy Simulation (LES), see next section.

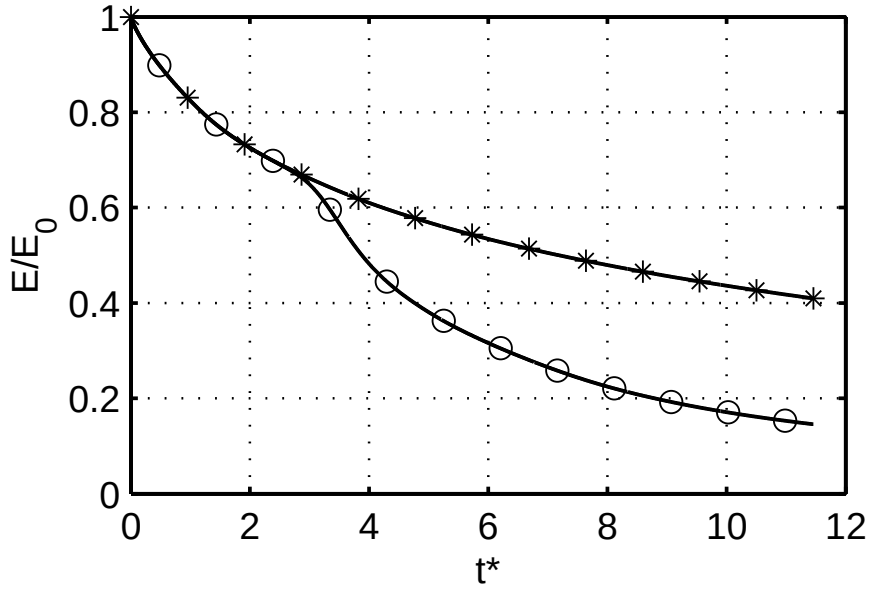

Figure 4: Evolution of the energy: 2-D ($*$) and 3-D ($\circ$) simulations.

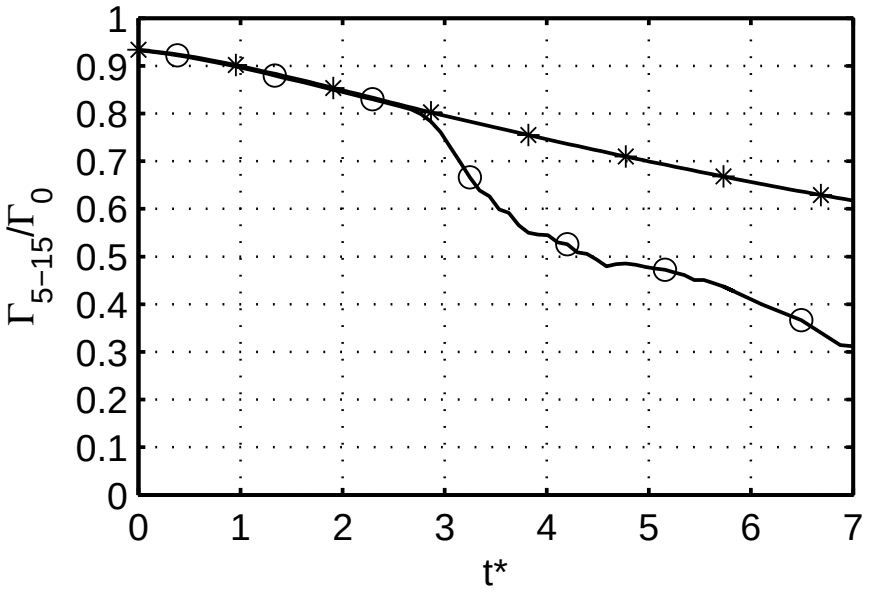

Figure 5: Evolution of the Γ_{5-15} circulation: 2-D ($*$) and 3-D ($\circ$) simulations.

3 LES AND SUBGRID SCALE MODELLING

As explained above, to simulate wake vortices from experiments at $Re > 5000$, and up to real aircraft conditions, requires LES. Concerning wakes in ground effects, it is also important to realize that "wall-resolved LES" (i.e., LES without "wall modelling") is still limited to, say, $Re = 50000$; LES at higher Reynolds number necessarily calls for additional, and "ad hoc", wall modelling.

We here only consider LES for wakes out of ground effects. LES at "very high Reynolds number" is also considered (i.e., turbulence where the SGS model dissipation is much higher than that due to molecular viscosity), see also [10]. Two types of subgrid scale (SGS) models are discussed: (1) models with diffusion operator acting on the complete LES field, using $\tau_{ij} = 2\,\nu_{\rm sgs}\,S_{ij}$ as subgrid stress model (where $S_{ij} = \frac{1}{2}\,(\partial u_i/\partial x_j + \partial u_j/\partial x_i)$ is the strain rate of the complete LES field) and (2) models with diffusion operator acting on the "small-scale" LES field, using instead $\tau_{ij} = 2\,\nu_{\rm sgs}\,S^s_{ij}$ (where S^s_{ij} is the strain rate of the small-scale LES field). In each category, the effective SGS viscosity itself can be evaluated using the complete field or the small-scale field.

The models with diffusion operator acting on the complete field are considered first. The classical Smagorinsky (SMAG) model is the most common model:

$$\tau_{ij} = 2\,C_S\,\Delta^2\,(2\,S_{kl}S_{kl})^{1/2}\;S_{ij} \tag{2}$$

where Δ is the LES cutoff size. For LES on a uniform grid, we use the grid size: $\Delta = h$; otherwise, it is evaluated using the local grid sizes, h_x, h_y and h_z: various approaches exists. The SMAG model is a "complete-complete" model. The theoretical value of its coefficient in isotropic turbulence at high Reynolds number and for LES cutting well into the inertial range (i.e., LES with $\Delta/\eta \geq 20$ where η is the Kolmogorov scale) is $C_S = (0.3)^3 = 0.027$. The Wall Adapting Local Eddy-viscosity (WALE) model of [11] constitutes a useful improvement of the SMAG model for wall-bounded (and wall-resolved) LES: the effective SGS viscosity is then rescaled so as to have the proper near-wall behavior.

The "small-complete" version of the SMAG model (SMAG2) corresponds to using instead

$$\tau_{ij} = 2\,C_{S2}\,\Delta^2\,(2\,S^s_{kl}S^s_{kl})^{1/2}\;S_{ij}\;. \tag{3}$$

This is then very similar to the "Filtered Structure Function" (FSF) model of [12]: also a "small-complete" model, but using

$$\tau_{ij} = 2\,C_{FSF}\,\Delta\,(F^s_2)^{1/2}\;\;S_{ij} \tag{4}$$

where F^s_2 is taken as

$$F^s_2 \;=\; \left\langle \| \,\mathbf{u}^s(\mathbf{x}+\mathbf{x}') - \mathbf{u}^s(\mathbf{x})\,\|^2 \right\rangle_{|\mathbf{x}'|\,=\,\Delta} \tag{5}$$

which is itself evaluated numerically using the nearest neighbors ($3^3 = 27$) values.

The small-scale field can be obtained efficiently using the compact (stencil 3) tensor-product discrete filter (eventually iterated n times) [13, 14]:

$$\mathbf{u}^s = \mathbf{u} - \overline{\mathbf{u}} \quad \text{with} \quad \overline{\mathbf{u}} = \Big[\Big(I - \Big(-\delta_x^2/4\Big)^n\Big)\Big(I - \Big(-\delta_y^2/4\Big)^n\Big)\Big(I - \Big(-\delta_z^2/4\Big)^n\Big)\Big]\,\mathbf{u} \tag{6}$$

where $\delta_x^2 f_{i,j,k} = f_{i+1,j,k} - 2f_{i,j,k} + f_{i-1,j,k}$, etc. In Fourrier space, the filtered field is then

$$\begin{aligned} \overline{\mathbf{u}}(\mathbf{k}) &= G^{(n)}(k_x h_x)\, G^{(n)}(k_y h_y)\, G^{(n)}(k_z h_z)\, \mathbf{u}(\mathbf{k}) \\ &= \Big(1 - \sin^{2n}(k_x h_x/2)\Big)\Big(1 - \sin^{2n}(k_y h_y/2)\Big)\Big(1 - \sin^{2n}(k_z h_z/2)\Big)\,\mathbf{u}(\mathbf{k})\ . \end{aligned} \tag{7}$$

Another way of producing a small-scale field is to use

$$\mathbf{u}^s = \Big(-\Big(\delta_x^2/4 + \delta_y^2/4 + \delta_z^2/4\Big)\Big)^n\,\mathbf{u}\,. \tag{8}$$

This is what is used in [12] for the FSF model. This is a bit easier than using the tensor-product discrete filter; yet the transfer function,

$$\mathbf{u}^s(\mathbf{k}) = \Big(\sin^2(k_x h_x/2) + \sin^2(k_y h_y/2) + \sin^2(k_z h_z/2)\Big)^n\,\mathbf{u}(\mathbf{k})\ , \tag{9}$$

is not as good at the high wavenumbers.

The models with diffusion operator acting on the small-scale field are considered next. The "variational multiscale" models of [15, 16], but efficiently obtained using the discrete filters above, are considered next. The "complete-small" version reads

$$\tau_{ij} = 2\,C_{RVM}\,\Delta^2\,(2\,S_{kl}S_{kl})^{1/2}\ S^s_{ij}\ . \tag{10}$$

It was first proposed and tested by [13, 14] and called the "regularized variational multi-scale" (RVM) model. It was then further proposed and tested by [17]. The "small-small" version (RVM2) reads

$$\tau_{ij} = 2\,C_{RVM2}\,\Delta^2\,(2\,S^s_{kl}S^s_{kl})^{1/2}\ S^s_{ij}\ . \tag{11}$$

It was also proposed and tested by [18, 19] (who called it the "high-pass filtered eddy-viscosity model"). In the same, way, they also proposed a "small-small" version of the FSF model (FSF2):

$$\tau_{ij} = 2\,C_{FSF2}\,\Delta\,(F_2^s)^{1/2}\ \ S^s_{ij}\ . \tag{12}$$

3.1 LES of a counter-rotating four vortex system at very high Reynolds number

LES of a four-vortex system was done using the vortex-in-cell method combined with the parallel fast multipole method (so as to efficiently obtain the "open domain" boundary conditions for the Poisson solver on the VIC grid: the so called VIC-PFM method, see [2, 3]). The outer principal vortices are characterized by their circulation Γ_1, their inner spacing b_1 and their effective core size radius r_{c_1}. The inner secondary pair is characterized

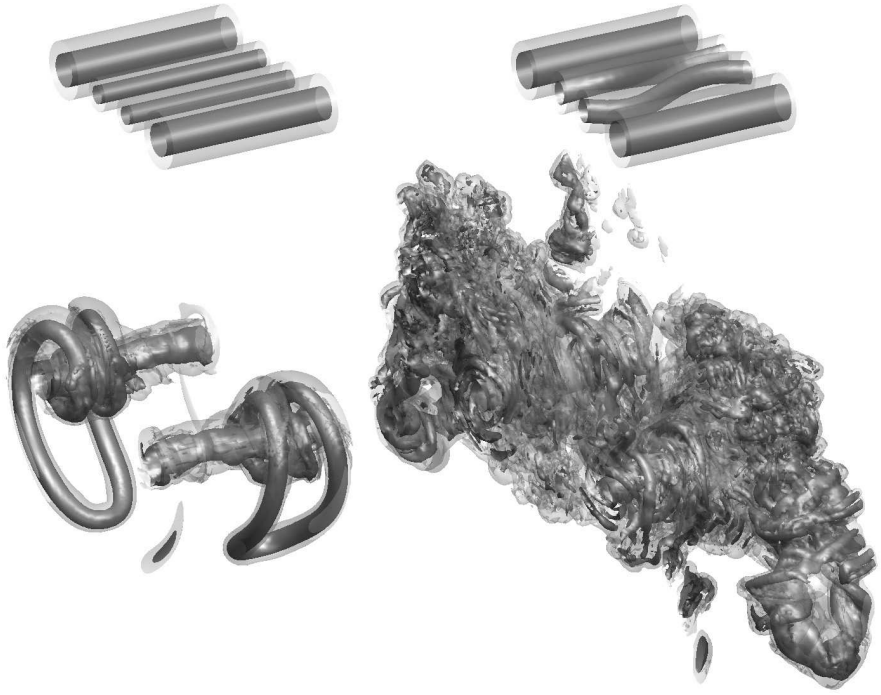

Figure 6: Evolution of the four-vortex system obtained using VIC-PFM with the RVM model. Isosurfaces shown are $|\boldsymbol{\omega}|b_1^2/\Gamma_1 = 10$ (high opacity) and 2 (low opacity). Times shown are $t^* = 0.0$, 0.61, 0.79 and 1.05 .

by Γ_2 , b_2 and r_{c_2} . We an algebraic distribution of circulation for each vortex. The global reference scales are $b_0 = (\Gamma_1 b_1 + \Gamma_2 b_2)/\Gamma_0$ with $\Gamma_0 = \Gamma_1 + \Gamma_2$, $V_0 = \Gamma_0/(2\pi\, b_0)$ and $t_0 = b_0/V_0$. All quantities can then be be written in dimensionless form (for instance, $t^* = t/t_0$). The case considered is $\Gamma_2/\Gamma_1 = -0.3$, $b_2/b_1 = 0.3$, $r_{c_1}/b_1 = 0.075$, and $r_{c_2}/r_{c_1} = 2/3$. This leads to $\Gamma_0/\Gamma_1 = 0.7$ and to $b_0/b_1 = 1.3$. The flow considered here is at very high Reynolds number and the LES was run without molecular viscosity (all the dissipation being provided by the SGS model). This configuration was shown to develop rapidly growing instabilities [20, 21, 3, 10]: the so-called "Omega loops". It thus provides a challenging simulation problem with rapid change in flow topology, generation of small scale structures (due to the incomplete reconnection between vortices of different strength) and, finally, turbulence. It was also used as a benchmark in the EC funded *AWIATOR* project, see [21]. The computational domain was taken as one period of the most unstable mode: $L_x/b_0 = 0.76$ ($L_x/b_1 = 0.99$). The grid was uniform and with resolution $h/b_1 = 0.0154$. The results using the RVM ($n = 3$) model is shown in Fig. 6 (see also [10]).

The multiscale models (RVM, RVM2, FSF, FSF2, SMAG2) all performed quite well: good energy conservation up to the time of strong vortex interactions, and then roughly same energy decay of the turbulent flow. The results shown are all $n = 3$; but even $n = 1$ produces results far superior to the SMAG or WALE models. The SMAG and the WALE

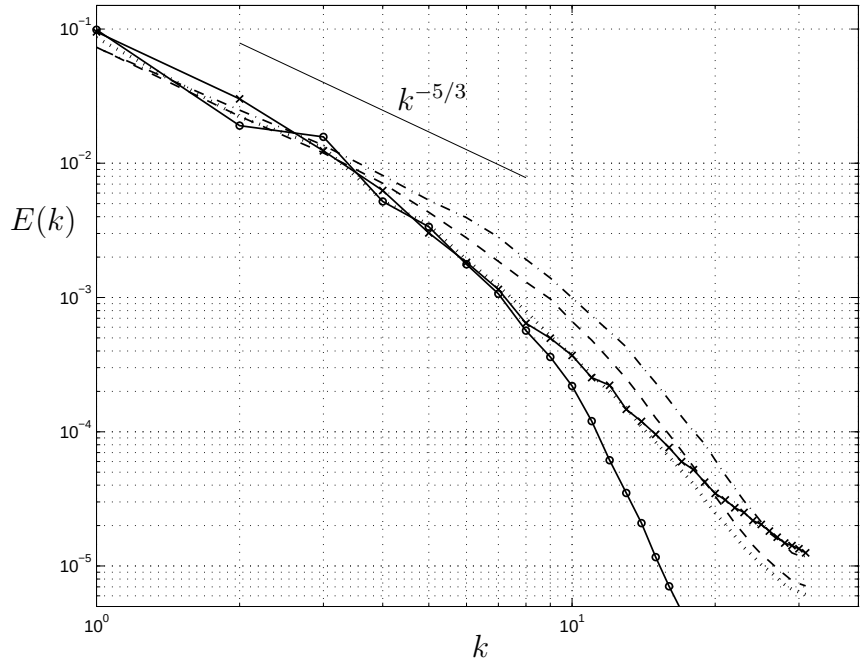

Figure 7: Energy spectrum at $t^* = 1.05$: SMAG (*dot*), RVM (*dash-dot*), FSF (*dash*), WALE (*solid with crosses*) and low order hyper-viscosity (*solid with circles*).

models are clearly not acceptable for LES of wake vortex flows. The spectral behavior of the models is shown in Figs. 7 and 8 which provide the spectrum of the turbulent flow. We confirm the good behavior of the multiscale models, best using the available wavenumbers of the LES grid: they preserve the low to medium wavenumbers (inertial range) while providing dissipation at the high wavenumbers. The SMAG and WALE models dissipate at all wavenumbers, thus significantly altering the inertial range dynamics of the LES.

We also note that the energy decay during the turbulent phase of the flow is essentially independent of the SGS model details, as long as the model is "good": i.e., that does not affect the large to medium scale dynamics. In turbulence, it is indeed the dynamics of those scales that determine the dissipation rate.

In order to better assess the potential of such four-vortex system, LES was also conducted at same resolution but over a much longer domain: $L_x/b_0 = 8.53$ $(L_x/b_1 = 11.1)$, see [10]. This also corresponds to one wavelength of the long, "Crow"-type, instability of the corresponding two-vortex system. The simulation was run using the VIC-PFM method on 48 processors, and up to $t^* = 1.50$. The VIC grid grew from $720 \times 128 \times 64$ to $720 \times 310 \times 312$ points and the number of vortex particles from 3.3 to 18 millions. This run was also done so as to compare with the results obtained using a Fourier-based spectral code run using a high order (k^8) hyper-viscosity SGS model and up to very long times: $t^* = 3.7$, which corresponds to a fully developed turbulent wake flow field. Of course, the spectral code assumes periodicity in all directions. The computational domain was

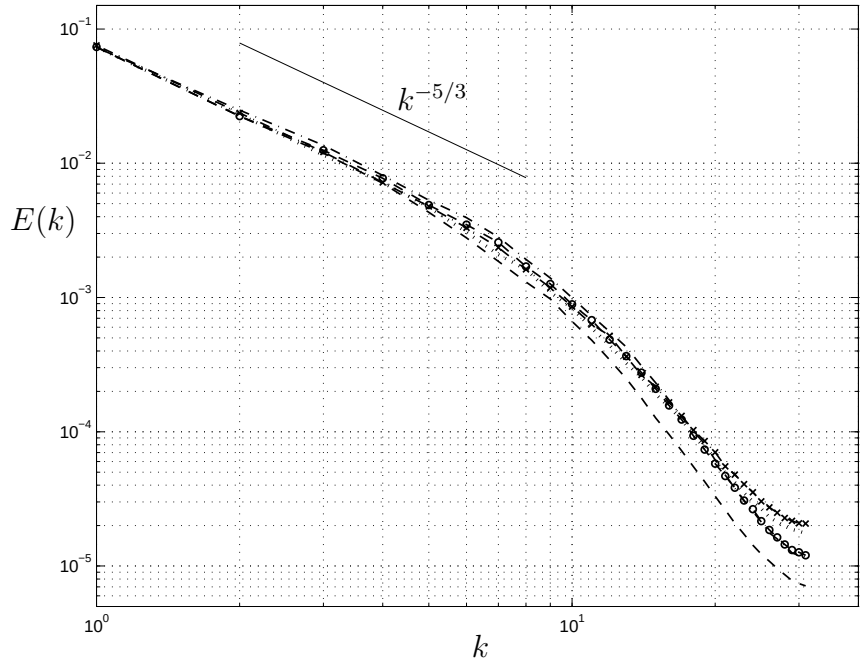

Figure 8: Energy spectrum at $t^* = 1.05$: SMAG2 (*dot*), RVM (*dash-dot*), RVM2 (*dash-dot with crosses*), FSF (*dash*) and FSF2 (*dash with circles*).

thus taken quite large: $720 \times 320 \times 224$ ($L_x/b_1 = 11.1$, $L_y/b_1 = 4.93$, $L_z/b_1 = 3.35$). The simulation was run on 20 processors. A global view of the results is shown in Fig. 9. The energy evolution is provided in Fig. 10. The net results is indeed a highly decayed turbulent vortex system. As to the VIC-PFM results, run up to $t^* = 1.50$, they indeed compared very well with the spectral results. The results of such simulations indicate that LES can indeed provide useful and quantitative information.

3.2 LES of isotropic turbulence at very high Reynolds number: further validation and calibration of the SGS models

The performance of the SGS models was also investigated in LES of decaying homogeneous isotropic turbulence at very high Reynolds number (i.e., only with SGS model dissipation), see [22]. This allowed for further assessment, validation and calibration on a flow with "a priori" known behavior.

Fig. 11 provides obtained energy spectra at two times (both taken when the LES field is statistically converged). We observe that the models acting on the complete field (thus at all scales), such as the SMAG model and the FSF model, are too diffusive at the medium scales and inside part of the inertial range. The multiscale models acting solely on the small-scale field, such as the RVM model, produce the best results: they allow to capture a significant inertial range, as their dissipation spectrum is mainly located at the large wavenumbers (and more so as n is taken larger). They are also verified to provide the best

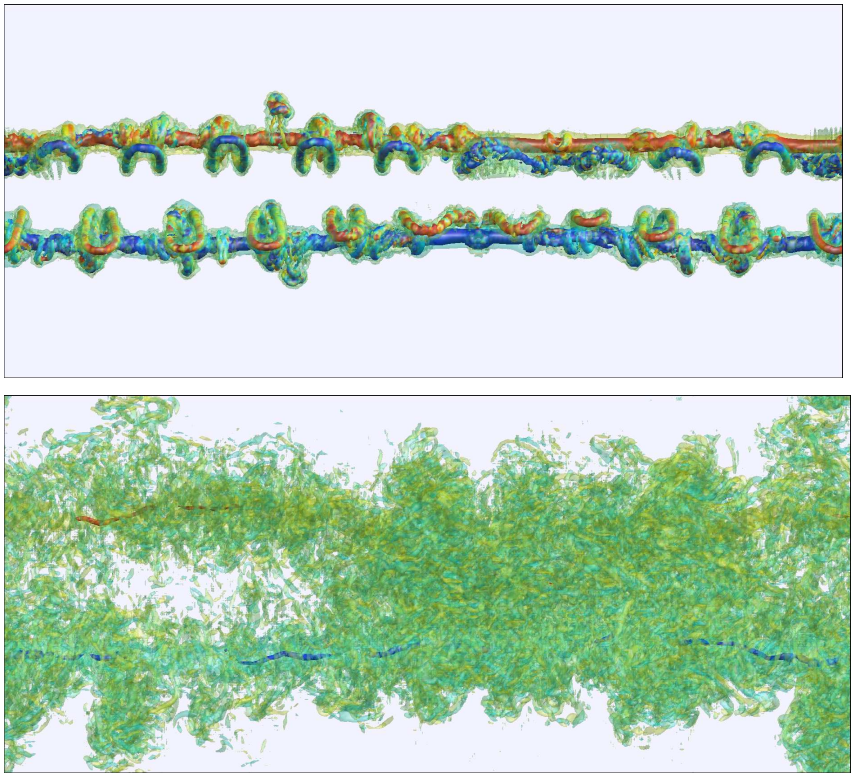

Figure 9: Visualization of the flow field at $t^* = 1.15$ and 3.7, using isosurfaces of $\|\vec{\omega}\| b_1^2/\Gamma_1 = 1$ and 10.

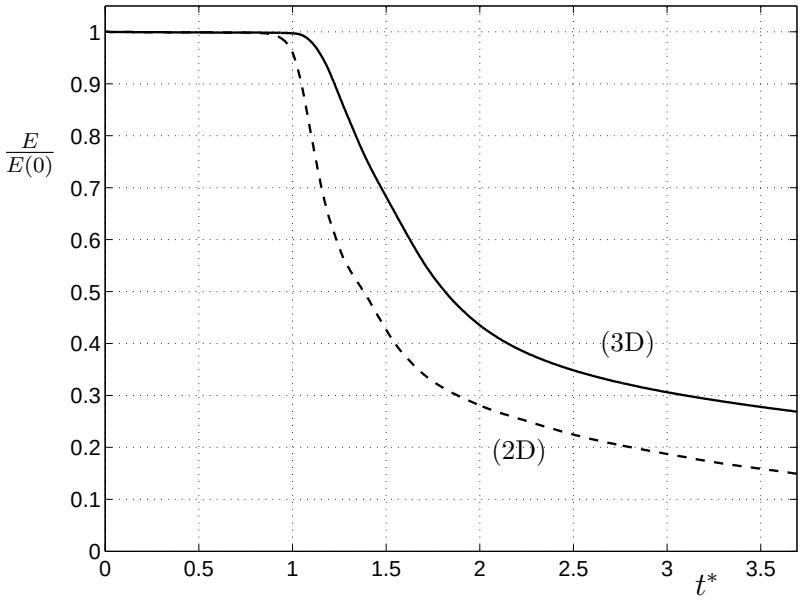

Figure 10: Evolution of the energy: complete field (solid) and longitudinally averaged field (dash). The difference is the turbulence energy.

C_S		0.027
C_{S2}	$(n=1)$	0.045
C_{FSF}	$(n=1)$	0.078
C_{RVM}	$(n=1)$	0.036
	$(n=3)$	0.060
C_{RVM2}	$(n=1)$	0.066
C_{FSF2}	$(n=1)$	0.110

Table 1: Values of the SGS model coefficients, as calibrated in homogeneous isotropic turbulence at very high Reynolds number.

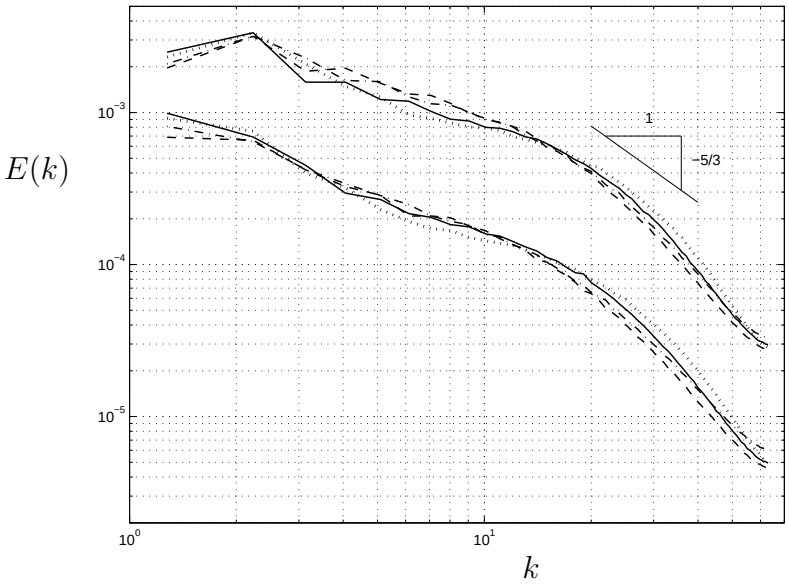

Figure 11: Energy spectra for decaying homogeneous isotropic turbulence, at two times: SMAG (*dash*), FSF (*dash-dot*), RVM with $n=1$ (*solid*) and RVM with $n=3$ (*dot*).

exponent for the asymptotic decay of turbulent energy, as t^{-p}: according to literature, p should lie in $[1.15, 1.45]$ ([23] suggesting that a good value is $p \approx 1.30$). The LES with RVM model (both $n = 1$ and $n = 3$) leads to a turbulence with decay exponent equal to $p = 1.38$. The models acting on the whole field produce spectra that are not as good, which, in turn, influence the obtained p value: $p = 1.49$ for SMAG (clearly out of range) and $p = 1.44$ for FSF (at the border of the range).

3.3 LES used to investigate the "equilibrium turbulent wake vortex system" at very high Reynolds number

LES can also serve to address the following question: what is the state of an "equilibrium turbulent wake vortex system" at very high Reynolds number? The present investigation was done using the spectral code. The results are still preliminary. The initial condition was taken as a vortex pair with algebraic circulation profile and $r_c/b_0 = 0.05$. The computational domain was $L = 4b_0$ in all directions. As the turbulent vortex system was the aim of the investigation, we did not allow for the long wavelength Crow instability; the domain was however taken large enough so as to minimize the effects of the periodic images. The size $4b_0$ is seen to be adequate. The mean energy of the base flow vortex system in the periodic domain, $E_{2D} = \frac{1}{L^2}\int_S \frac{(u^2+v^2)}{2}\, dS$, is then obtained as $E_{2D} = 0.947\, V_0^2$. The same vortex system in an unbounded domain has a total energy of

$$\begin{aligned} \tilde{E}_{2D} = \int_{S_\infty} \frac{(u^2+v^2)}{2}\, dS &= \frac{\Gamma_0^2}{2\pi}\left(\log\left(\frac{b_0}{r_c}\right) - \frac{1}{2}\right) = 2\pi\, b_0^2\, V_0^2\, \left(\log\left(\frac{b_0}{r_c}\right) - \frac{1}{2}\right) \\ &= 15.68\, b_0^2\, V_0^2 = 0.980\, L^2\, V_0^2\ . \end{aligned} \tag{13}$$

The difference in energy is thus small (of the order of 3-4%), indicative that the size of the computational domain is indeed acceptable.

We used 256^3 grid points (thus a spatial resolution of $h/b_0 = 0.0156$) and the simulation was run on 16 processors. The vortex system was initially perturbed, by putting it in an isotropic turbulence field (itself obtained by a previous LES) at very low energy (much lower than that of the base flow vortex system: 0.004 compared to 0.947). The system then evolved, through LES, to what essentially amounts to a "turbulent vortex system in equilibrium" (here achieved for $t^* \geq 4.5$). The evolution of the energy is provided in Fig. 12 and that of the modal energies in Fig. 13. As soon as the turbulent vortex is developed, the 3-D field energy E^* (defining $E^* = E/V_0^2$) and the longitudinally averaged field (base flow) energy E^*_{2D} decay at almost the same rate. This implies that the turbulent kinetic energy, which corresponds to the difference, remains roughly constant, indicative of equilibrium: base flow energy is constantly being transformed into turbulent energy and this compensates for the turbulence dissipation (here ensured by the SGS model). A view of the obtained turbulent vortex system is provided in Fig. 14. The base flow energy decay can also be related to each vortex global circulation decay; there is indeed some vorticity exchange through the mid plane, due to the turbulence.

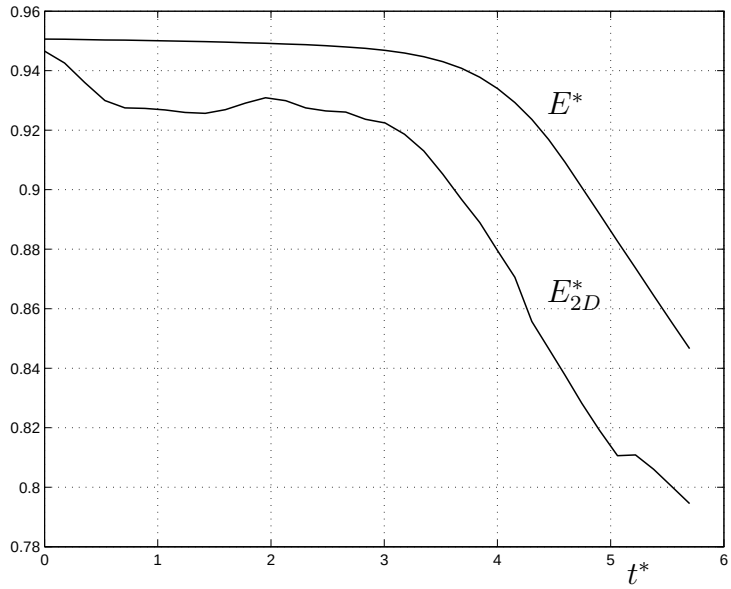

Figure 12: Evolution of the energy: complete field and longitudinally averaged field (base flow). The difference is the turbulent energy.

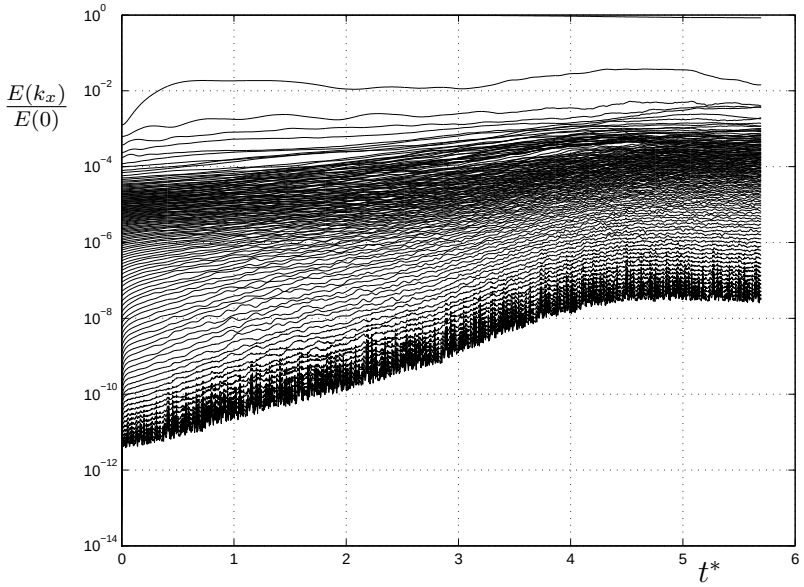

Figure 13: Evolution of the modal energies: from $k_x = 0$ (base flow) to $k_x = 127$.

The detailed analysis of the results is still ongoing work: characterization of the turbulence, quantification of the base flow energy and circulation decay rates, etc. Further validation of the results, as obtained by such LES, will also be required: LES using another initial condition (e.g., starting from more compact vortices), another SGS model (RVM2), another grid (finer), another code. Nevertheless, we believe that the present results are already quite good and are of some quantitative value.

Finally, we stress that, for a real turbulent vortex system, the Crow instability (on purpose not permitted in our simulation) will eventually be excited, and the turbulent vortex system will then decay much faster, through vortex reconnection, formation of turbulent vortex rings, etc.

4 CONCLUSION

Wake vortex flows are fascinating and very challenging to simulate: they constitute large scale problems that contain vortices with small cores and, most often, turbulence. Nowadays, the state-of-the art numerical methods, subgrid-scale models and computational ressources (also parallel computing) can be put to good use to simulate such flows. We have illustrated, through examples within our research group, what can be done in DNS and LES of such flows. The particular case of LES at very high Reynolds number, which is relevant to wakes produced by real aircraft, was also discussed, and some related LES results were presented. Of course, all this still requires further work and validation. Yet, the results obtained so far are already of quantitative value. The LES methodologies presented here were also used in recent EC funded projects, such as the *AWIATOR* project [21, 24] (results not shown here). In particular LES started from near wake experimental fields (wind tunnel data at $x/b = 0.5$) were shown to compare well with the experimental data measured further downstream (at $x/b = 6$ and 15): proper rollup and dynamics of the wake, including unstable 3-D vortex mergings, etc. This is indicative that a lot was already "right" in those LES, even though they corresponds to necessarily high truncation (e.g., only 6 to 8 grid points across one vortex core diameter).

5 ACKNOWLEDGEMENTS

The work was partially funded by EC projects: AWIATOR (*Aircraft WIng with Advanced Technology Operation*, IP of FP5, contract G4RD-CT-2002-00836) and FAR-Wake (*Fundamental Research on Aircraft Wake Phenomena*, STREP of FP6, contract AST4-CT-2005-012238).

REFERENCES

[1] O.V. Vasilyev, High order finite difference schemes on non-uniform meshes with good conservation properties, *J. Comp. Phys.*, **157**(2): 746–761 (2000).

[2] G. S. Winckelmans, Chapter 5: *Vortex Methods*, in Volume 3 (Fluids) of the *Encyclopedia of Computational Mechanics*, Erwin Stein, René de Borst, Thomas J. R.

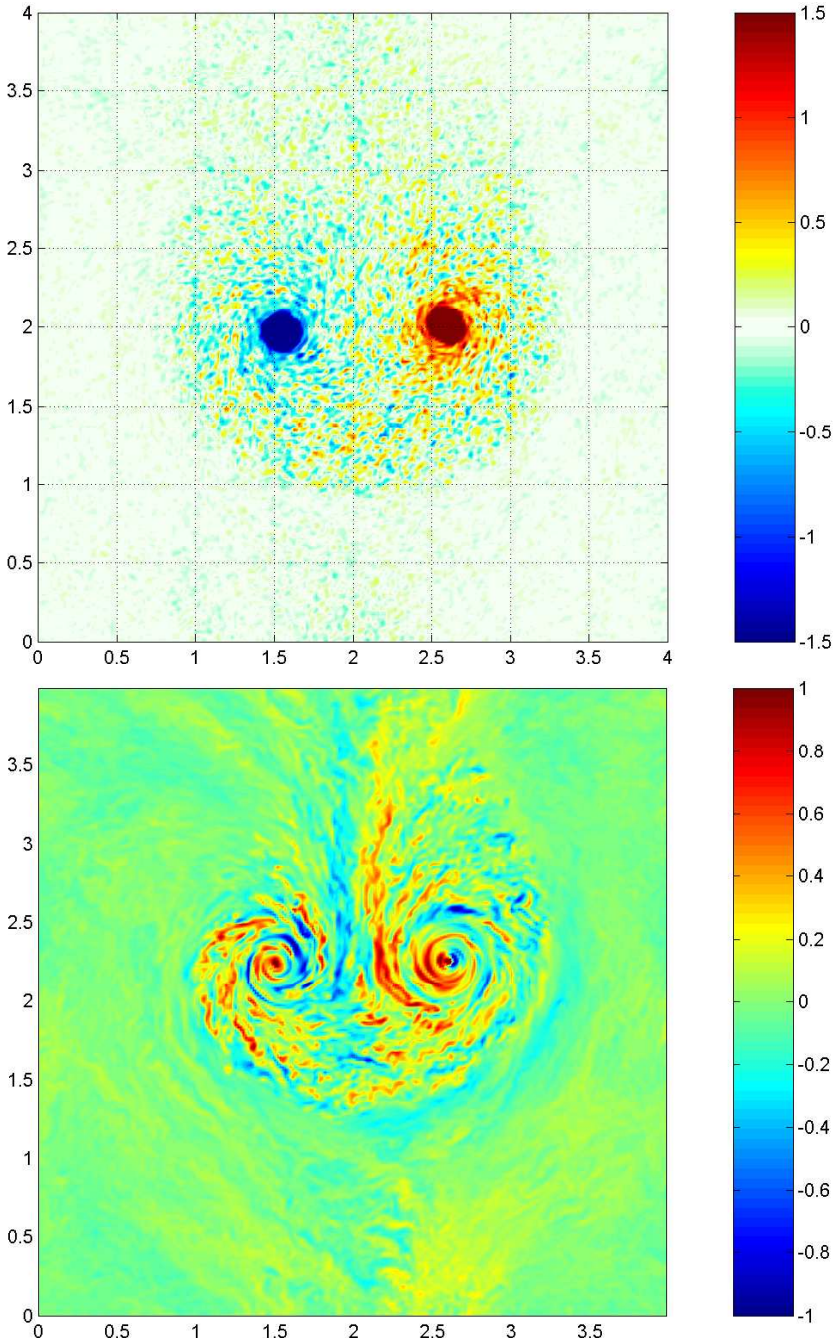

Figure 14: Visualization of the equilibrium turbulent vortex system ($t^* = 5.06$). Top: axial vorticity, $\omega\, b_0^2/\Gamma_0$, of the base flow (figure highly saturated to show the vorticity outside the cores, indeed $\omega_{\max}\, b_0^2/\Gamma_0 = 127.3$). Bottom: axial velocity, u/V_0, for a cut through the flow field (recall that the axial velocity of the base flow is zero).

Hughes (Eds), John Wiley & Sons, 2004.

[3] G. Winckelmans, R. Cocle, L. Dufresne and R. Capart, Vortex methods and their application to trailing wake vortex simulations, *C. R. Physique* (Académie des Sciences, Paris, special issue on *Aircraft trailing vortices*), **6**(4-5): 467-486 (2005).

[4] T. Leweke and C. H. K. Williamson, Cooperative elliptic instability of a vortex pair, *J. Fluid. Mech.*, **360**: 85–119 (1998).

[5] M. Duponcheel, T. Lonfils, L. Bricteux and G. Winckelmans, Simulation of three-dimensional wake vortices in ground effect using a fourth order incompressible code, Proc. *7th National Congress on Theoretical and Applied Mechanics* (NCTAM2006, organised by the National Committee for Theoretical and Applied Mechanics), Mons, Belgium, May 29–30, 2006.

[6] J.A. Luton and S.A. Ragab, Three-dimensional interaction of a vortex pair with a wall, *Phys. Fluids*, **9**(10): 2967–2980 (1997).

[7] S.E. Widnall, D.B. Bliss, and C.Y. Tsai, The instability of short waves on a vortex ring, *J. Fluid Mech.*, **66**: 35–47 (1974).

[8] F. H. Proctor, D. W. Hamilton, and J. Han, Wake vortex transport and decay in ground effect: Vortex linking with the ground, *38th AIAA Aerospace Sciences Meeting & Exhibit*, Reno, NV, Jan. 10–13 2000, paper AIAA 2000–0757.

[9] F. Holzäpfel and M. Steen, Aircraft wake-vortex evolution in ground effect: Analysis and parameterization, *44th AIAA Aerospace Sciences Meeting & Exhibit*, Reno, NV, Jan. 9–12 2006, paper AIAA 2006–1077.

[10] R. Cocle, L. Dufresne and G. Winckelmans, Investigation of multiscale subgrid models for LES of instabilities and turbulence in wake vortex systems, Lecture Notes in Computational Science and Engineering series, Symposium on *Complex Effects in Large Eddy Simulation (CY-LES 2005)*, Springer, to appear 2006.

[11] F. Nicoud and F. Ducros, Subgrid-scale stress modelling based on the square of the velocity gradient tensor, *Flow Turb. Comb.*, **62**(3): 183–200 (1999).

[12] F. Ducros, P. Comte and M. Lesieur, Large-eddy simulation of transition to turbulence in a boundary layer spatially developing over a flat plate, *J. Fluid Mech.*, **326**: 1–36 (1996).

[13] G. S. Winckelmans and H. Jeanmart, Assessment of some models for LES without and with explicit filtering, *Direct and Large-Eddy Simulation IV*, edited by Geurts B.J., Friedrich R. and Métais O., ERCOFTAC Series **8**, Kluwer, 55–66 (2001).

[14] H. Jeanmart and G. S. Winckelmans, Comparison of recent dynamic subgrid-scale models in turbulent channel flow, Proc. *Summer Program 2002*, Center for Turbulence Research, Stanford University and NASA Ames, 105–116 (2002).

[15] T. J.R. Hugues, L. Mazzei , A. A. Oberai and A. A. Wray, The multiscale formulation of large eddy simulation: decay of homogeneous isotropic turbulence, *Phys. Fluids*, **13**: 505–512 (2001).

[16] T. J.R. Hugues, A. A. Oberai and L. Mazzei, Large eddy simulation of turbulent channel flow by the variational multiscale method, *Phys. Fluids*, **13**: 1784–1799 (2001).

[17] A.W. Vreman, The filtering analog of the variational multiscale method in large-eddy simulation, *Phys. Fluids*, **15**, L61 (2003).

[18] S. Stolz, P. Schlatter , D. Meyer and L. Kleiser, High-pass filtered eddy-viscosity models for LES, *Direct and Large-Eddy Simulation V*, edited by Friedrich R., Geurts B.J. and Métais O., Kluwer, 81–88 (2004).

[19] S. Stolz, P. Schlatter and L. Kleiser, High-pass filtered eddy-viscosity models for large-eddy simulations of transitional flow, *Phys. Fluids*, **17**, 065103:1–14 (2005).

[20] D. Fabre, L. Jacquin and A. Loof, Optimal perturbations in a four-vortex aircraft wake in counter-rotating configuration, *J. Fluid Mech.*, **451**, 319–328 (2002).

[21] L. Dufresne, R. Capart and G. Winckelmans, *Report of benchmark study*, AWIATOR final report D1.1.4-16, 2005. (Also to be submitted as paper: L. Dufresne, R. Baumann, T. Gerz, G. Winckelmans, H. Moet, R. Capart and L. Nybelen, Large-eddy simulation of wake vortex flows at very high Reynolds numbers: a comparison of different methodologies).

[22] R. Cocle and G. Winckelmans, Investigation of multiscale subgrid-scale models in homogeneous isotropic turbulence at high Reynolds number, Proc. *7th National Congress on Theoretical and Applied Mechanics* (NCTAM2006), Mons, Belgium, May 29–30, 2006.

[23] M. S. Mohamed and J. C. LaRue, The decay power law in grid-generated turbulence, *J. Fluid Mech.*, **219**: 195–214 (1990).

[24] L. Dufresne, R. Capart, G. Winckelmans and O. Desenfans, *Analysis report: Flow topology aspects*, AWIATOR final report D1.1.4-7, 2006.